

# Optics Letters

## Single-frequency Tm-doped fiber laser with 215 mW at 2.05 $\mu\text{m}$ based on a Tm/Ho-codoped fiber saturable absorber

LU ZHANG,<sup>1,2</sup> QUAN SHENG,<sup>1,2,\*</sup> LIN CHEN,<sup>3</sup> JUNXIANG ZHANG,<sup>1,2</sup> SHIJIE FU,<sup>1,2</sup> QIANG FANG,<sup>4</sup> YIPING WANG,<sup>3</sup> WEI SHI,<sup>1,2,5</sup> AND JIANQUAN YAO<sup>1,2,6</sup>

<sup>1</sup>Institute of Laser and Optoelectronics, School of Precision Instrument and Optoelectronics Engineering, Tianjin University, Tianjin 300072, China

<sup>2</sup>Key Laboratory of Opto-electronic Information Technology, Ministry of Education, Tianjin University, Tianjin, 300072, China

<sup>3</sup>Key Laboratory of Optoelectronic Devices and Systems of Ministry of Education and Guangdong Province, College of Optoelectronic Engineering, Shenzhen University, Shenzhen 518060, China

<sup>4</sup>HFB Photonics Co. Ltd., Weihai, Shandong, 264209, China

<sup>5</sup>e-mail: shiwei@tju.edu.cn

<sup>6</sup>e-mail: ypwang@szu.edu.cn

\*Corresponding author: shengquan@tju.edu.cn

Received 6 May 2022; revised 4 July 2022; accepted 13 July 2022; posted 14 July 2022; published 29 July 2022

We demonstrate an efficient single-frequency Tm-doped fiber laser at 2050 nm. A ring cavity scheme is employed to boost the net gain at the wavelength. A piece of Tm/Ho-codoped fiber with an absorption coefficient at 2050 nm higher than that of a Tm-doped fiber is used to establish the dynamic Bragg grating for enhancing the frequency selection capability. A single-frequency output of 215 mW is obtained under 2 W of 1570-nm pump power, with the slope efficiency being 22%. To the best of our knowledge, this is the highest single-frequency all-fiber laser oscillator output power above 2  $\mu\text{m}$ . © 2022 Optica Publishing Group

<https://doi.org/10.1364/OL.463202>

Single-frequency fiber laser sources operating in the wavelength region of 2.05  $\mu\text{m}$ , where CO<sub>2</sub> has a strong absorption, are widely used in coherent Doppler LIDAR and differential absorption LIDAR, atmospheric analysis, and spectral sensing [1–3]. Over the past decades, several schemes have been employed to realize single-frequency operation in fiber lasers, such as the short linear cavity fiber lasers with distributed feedback (DFB) and distributed Bragg reflector (DBR) structure. The output power and efficiency of the 2- $\mu\text{m}$  single-frequency fiber lasers have been improved rapidly by using a heavily Tm-doped germanate fiber [4]. However, the laser wavelengths of the previous reports are usually below 2000 nm and achieving an efficient single-frequency fiber laser at longer wavelength is still challenging [5]. The combination of the diminishing emission cross section of Tm<sup>3+</sup> above 2  $\mu\text{m}$  and the limited laser gain provided by the short Tm-doped fiber means the conventional DBR or DFB Tm-doped fiber lasers are not applicable in this wavelength region. To the best of our knowledge, to date, the maximum single-frequency oscillator output power at 2.05  $\mu\text{m}$  is only 65 mW, which was obtained from a DFB Tm-doped fiber laser demonstrated in 2021 [6]. The

slope efficiency with respect to the 1550-nm pump power is only 8.5%.

An alternative is the ring cavity fiber lasers. This scheme allows the optimization of the active fiber length to improve the pump absorption and laser gain for a higher output power [7–9]. By further incorporating a piece of rare-earth-doped fiber based saturable absorber (SA) as well as a high reflectivity mirror or fiber Bragg grating (FBG), a narrow bandwidth dynamic Bragg grating would be established inside the SA based on the standing-wave interference effect, forcing the intracavity laser to operate in a single longitudinal mode scheme. In addition, the saturable absorption process in the SA would introduce a frequency-dependent loss. The weak longitudinal modes, which deviate the center frequency, would undergo a larger absorption loss and can be effectively suppressed owing to the mode competition [10]. It has been demonstrated that using a highly absorptive fiber SA would enhance the strength of the dynamic Bragg grating and the absorption loss [11], resulting in a strong mode selection capability. This could be achieved by using a heavily doped fiber. However, the bandwidth of the induced dynamic Bragg grating would become broader as the doping concentration increases, which will result in severe mode-hopping [12]. In contrast, using a low/moderate dopant fiber, the doped rare-earth ions, which have a large absorption cross section at the signal wavelength, would induce a strong dynamic Bragg grating with narrower bandwidth, and thus is more beneficial for stable and powerful single-frequency operation. However, in the previous demonstrations of single-frequency fiber lasers above 2  $\mu\text{m}$  with such a scheme, all the SAs used are Tm-doped fibers [13–15]. Limited by the weak mode selection resulting from the low absorption of Tm<sup>3+</sup> ions in this wavelength region, the maximum single-frequency power is only 40 mW [16].

Here, we propose an alternative approach that uses a Tm/Ho-codoped fiber as the SA to achieve single-frequency operation at 2.05  $\mu\text{m}$ . The absorption cross section (@ 2050nm) of

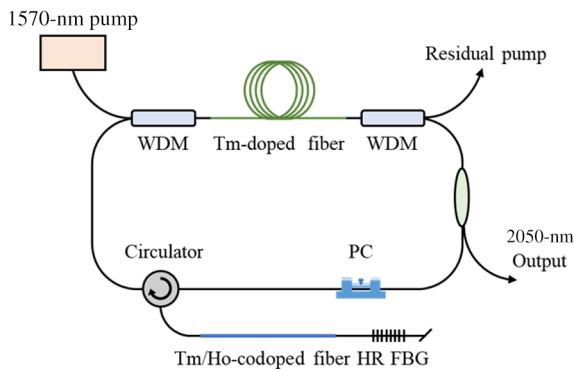


**Fig. 1.** Schematic of the 2.05- $\mu\text{m}$  single-frequency Tm-doped fiber ring laser. PC, polarization controller.

$\text{Ho}^{3+}$  ions is approximately  $0.6 \times 10^{-25} \text{ m}^2$  [17], and is much larger than that of the  $\text{Tm}^{3+}$  ions ( $< 0.1 \times 10^{-25} \text{ m}^2$ ). Therefore, compared with the singly Tm-doped fiber SA, the introduction of  $\text{Ho}^{3+}$  ions would enhance the saturable absorption process and lead to a stronger dynamic Bragg grating. By optimizing the length of Tm/Ho-codoped fiber SA, over 200 mW of stable single-frequency laser at 2.05  $\mu\text{m}$  is obtained. Furthermore, a comparative experiment that uses a single Tm-doped fiber as the SA is also conducted. The results highlight the significant improvement of single-frequency output power resulting from the  $\text{Ho}^{3+}$  ions.

The experimental setup of the 2.05- $\mu\text{m}$  single-frequency Tm-doped fiber laser is depicted in Fig. 1. The pump source is a 1570-nm Er/Yb-codoped fiber laser providing a maximum output power of approximately 8 W. The gain medium is a piece of Tm-doped silica fiber (Nufern, SM-TSF-9/125) with an absorption coefficient at 1570 nm of 6 dB/m. Due to the reabsorption loss at 2050 nm in the Tm-doped fiber being neglectable, a 5-m Tm-doped fiber is used to ensure a sufficient pump absorption. Two 1570/2050-nm filtered wavelength division multiplexers (FWMs) are used to couple the pump power into the Tm-doped fiber and remove the residual pump power. A fused fiber coupler is spliced after the WDM to serve as the output element. The previous calculation shows that a large output coupling is beneficial for an efficient laser output. However, this would decrease the stability of the single-frequency laser due to only a small part of the intracavity lasing being able to return to the SA and the consequent weak dynamic Bragg grating. Therefore, a moderate output coupling of  $\sim 60\%$  is employed to balance the trade-off between the high output power and laser stability. A circulator is used to force the intracavity laser to be unidirectional traveling. The central laser wavelength is determined by a 2050-nm high-reflectivity FBG ( $R > 99.5\%$ ) with a 3-dB bandwidth of 0.2 nm. The FBG is written in a standard single-mode fiber (Corning, SMF-28e). The end-faces of the FBG fiber and WDM fiber are cleaved at an angle of  $8^\circ$  to reduce the Fresnel reflection feedback.

Without the Tm/Ho-codoped fiber SA, the 2050-nm output power as a function of the launched 1570-nm pump power was first measured and is shown in Fig. 2(a). The laser threshold was approximately 0.9 W. As the pump power increased, the 2050-nm output power exhibited a linear rise with a slope efficiency of 25.6%. When the launched 1570-nm pump power was 7.5 W, a maximum output power of 1.72 W was obtained. The low efficiency and output power are attributed to the limited

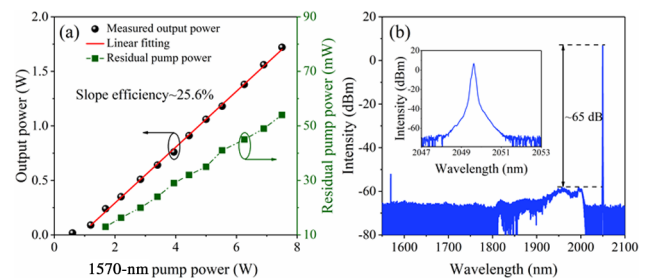


**Fig. 2.** (a) Measured 2050-nm output power as a function of the launched 1570-nm pump power, (b) laser spectrum at a maximum output power of 1.72 W. Inset shows the zoomed-in spectrum. The green dashed line in panel (a) is shown as a visual guide.

laser gain of the Tm-doped fiber at 2.05  $\mu\text{m}$  as well as the high background transmission loss of the silica fiber above 2  $\mu\text{m}$ . The residual pump power is also shown in Fig. 2(a). Due to the usage of a relatively long Tm-doped fiber, the residual pump power was below 60 mW at the maximum pump power, indicating a sufficient pump absorption above 20 dB. The laser spectrum at the maximum output power was recorded by the optical spectrum analyzer (OSA, AQ6375) with a resolution of 50 pm. As shown in Fig. 2(b), the center wavelength, full width at half maximum (FWHM), and optical signal-to-noise ratio (OSNR) of the output laser was 2049.62 nm, 75 pm, and 65 dB, respectively. Due to the sufficient pump absorption and the usage of a filtered-type WDM, there was very little of the 1570-nm pump in the output laser.

Then, a 4-m Tm/Ho-codoped fiber (Coractive, TH512) serving as the SA was inserted between the circulator and FBG for a fine longitudinal mode selection. The core absorption coefficient at 2050 nm was experimentally measured as approximately 0.97 dB/m with the cut-back method at the launched 2050-nm power of 80 mW. To enhance the intensity of the dynamic Bragg grating, a polarization controller (PC) was placed before the circulator to adjust the polarization state of the laser launched into the SA for a strong interference. The total cavity length was approximately 21 m, corresponding to a longitudinal mode spacing of 9.8 MHz. The longitudinal mode characteristics of the output laser were measured synchronously by a scanning Fabry–Perot interferometer (FPI) (Thorlabs, SA210-12B) and an electrical spectrum analyzer (Agilent Inc., PXA N9030A). The resolution and free spectra range of FPI were 67 MHz and 10 GHz, respectively. The radio frequency (RF) spectrum and oscilloscope trace at different pump powers are shown in Fig. 3. At lower pump power, there was only one longitudinal mode within a scanning cycle and no beat signal was observed in the RF spectrum within a frequency range of 0–100 MHz, indicating that the laser was operating in a stable and mode-hopping-free single-frequency scheme. By carefully adjusting the PC, a maximum single-frequency output power of 215 mW was obtained at 2.02-W pump power. As the pump power was further increased, more longitudinal modes started oscillating, weakening the standing-wave interference in the SA. In turn, this would wash out the dynamic Bragg grating. As a result, the single longitudinal mode trace turned to a broad envelope with a FWHM of approximately 3 GHz ( $\sim 42 \text{ pm}$  @ 2050 nm) [see inset in Fig. 3(b)]. Due to the beating of dense longitudinal modes, a periodic beat signal was observed in the RF spectrum. The frequency spacing of the neighboring beat signal was 9.6 MHz,

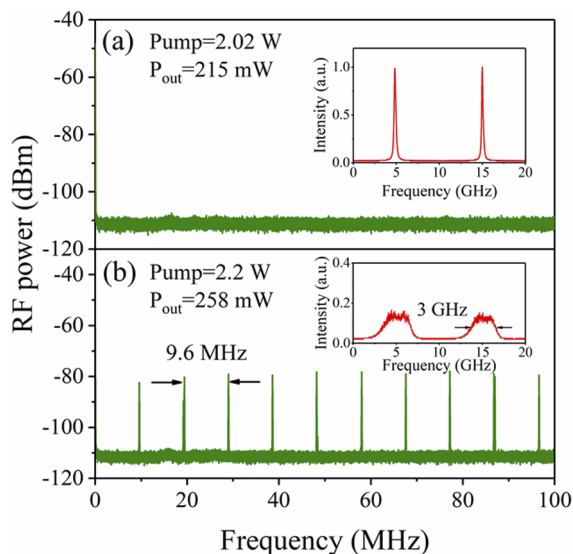


**Fig. 3.** RF spectrum and oscilloscope trace of the FP interferometer at launched 1570-nm pump powers of (a) 2.02 W and (b) 2.2 W.

agreeing well with the longitudinal mode spacing of the ring cavity.

Note that the length of the SA is an important parameter determining its mode selection capability. Since the bandwidth of dynamic Bragg grating is inversely proportional to its length, a longer SA generally has a narrow bandwidth and thus is more beneficial for stable single longitudinal mode operation. Here, the power behavior of a 2050-nm single-frequency laser with different Tm/Ho-codoped fiber SA length is investigated and the results are shown in Fig. 4(a). Since the SA induced an additional absorption loss, the slope efficiency decreased while the laser threshold increased. Such deterioration would become more severe with a longer SA due to an increasing cavity loss. When the SA length was 2 m, the single-frequency operation could be realized at a pump power of no more than 1.6 W. The maximum single-frequency output power was approximately 160 mW with a slope efficiency of 24%. As the SA length was increased to 4 m, the maximum single-frequency output power was scaled up to 215 mW at a pump power of 2.02 W, corresponding to a slope efficiency of 22%. As the SA length was further increased to 6 m, the maximum pump power allowing single-frequency operation increased to 2.2 W. It was found that a longer SA allowed single-frequency oscillation at a higher pump power. However, the maximum single-frequency power decreased to 180 mW due to the drop of the slope efficiency. In addition, a longer SA will enlarge the cavity length and reduce the longitudinal mode spacing, which also hinders the stable single longitudinal mode operation. Therefore, for the single-frequency fiber lasers based on a SA, a trade-off between high laser efficiency and strong frequency selection requires careful consideration, i.e., optimizing the SA length, for a powerful and stable single-frequency output. In the current experiment, the optimal Tm/Ho-codoped fiber length is approximately 4 m and the following laser characteristics were measured under this condition.

Figure 4(b) shows the laser spectrum at an output power of 215 mW, and the output spectrum without SA at the same pump

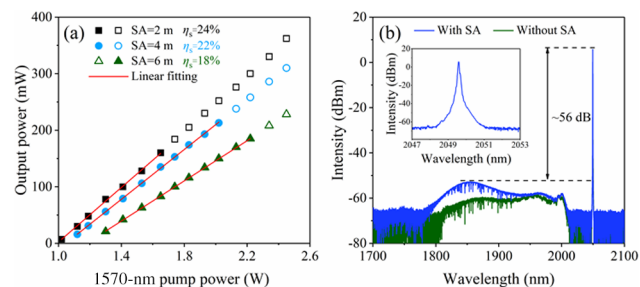


**Fig. 4.** (a) Measured 2050-nm output power as a function of the launched 1570-nm pump power with different Tm/Ho-codoped fiber lengths, (b) laser spectrum with and without SA. Inset shows the zoomed-in laser spectrum. The solid and hollow symbols in panel (a) represent the single-frequency and multi-longitudinal-mode operation, respectively.

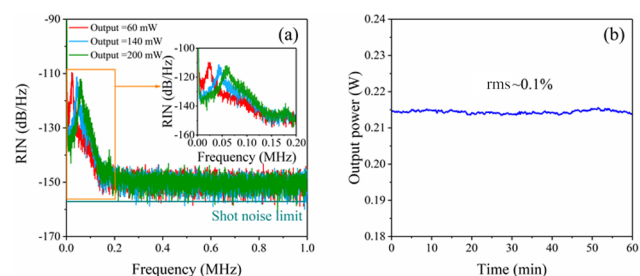


**Fig. 5.** (a) RIN of the 2050-nm single-frequency fiber laser at different pump powers, (b) power stability over one hour. Inset shows the zoomed-in RIN.

level is also given for comparison. A severe amplified spontaneous emission (ASE) envelope in the range of 1800–2000 nm was observed after the introduction of the SA. This can be explained as follows. The introduction of the SA decreases the intracavity signal power, which induces the generation of short-wavelength ASE and thus decreases the OSNR to 56 dB. Higher cavity feedback can be used to further improve the OSNR. The inset shows the zoomed-in spectrum of the 2050-nm single-frequency laser. Limited by the resolution of the OSA, the FWHM was measured to be approximately 0.05 nm.

The relative intensity noise (RIN) of the 2050-nm single-frequency fiber laser was measured by the electrical spectrum analyzer with a bandwidth resolution of 1 kHz. The power of the 2050-nm single-frequency laser launched into the photoelectric detector was attenuated to 1 mW, corresponding to a shot noise limit of  $-157.1$  dB/Hz. The measured RIN at different pump powers are shown in Fig. 5(a). Compared with the conventional DFB or DBR short-cavity single-frequency fiber lasers, the demonstrated fiber ring laser has a much lower relaxation oscillation frequency (ROF). As the pump power was increased from 1.3 W to 1.95 W (output power increasing from 60 mW to 200 mW), the ROF moved to a higher frequency from 23.5 kHz to 58.5 kHz, and the intensity decreased from  $-109.3$  dB/Hz to  $-112.3$  dB/Hz. The inset shows the zoomed-in RIN in the range of 0–0.2 MHz. In addition to the relaxation oscillation peak, it is noticed that there is also a broad peak at approximately 0.1 MHz. The center frequency of this broad peak is constant. Actually, in our previous work (the pump source used is the same one), a similar peak was also observed at the same frequency. Hence, we conjecture that this broad peak was also

**Table 1. Single-frequency Laser Power at 2050 nm (and the Corresponding Pump Power) with Different SA Lengths**

	2 m	4 m	6 m
Tm-doped fiber	/ (/)	60 mW (1.23 W)	93 mW (1.4 W)
Tm/Ho-codoped fiber	160 mW (1.65 W)	215 mW (2.02 W)	180 mW (2.2 W)

noise from the 1570-nm pump source [12,17]. At a higher frequency beyond the ROF, the RIN intensity dropped dramatically and became stable at approximately  $-150$  dB/Hz. The low noise intensity resulted from the high-brightness core-pump scheme and high-performance pump source with a high stability for power and wavelength. To characterize the power stability of the 2050-nm single-frequency fiber laser, the output power was monitored over one hour by a thermal power meter at an output of 215 mW. As shown in Fig. 5(b), the root mean square (rms) for the output power was approximately 0.1%, confirming a stable single-frequency operation.

To study the difference in mode selection capabilities of the Tm-doped fiber and Tm/Ho-codoped fiber in the 2.05- $\mu$ m wavelength region, the output laser characteristics using a Tm-doped fiber as the SA were also experimentally investigated. Here, the Tm-doped fiber used was chosen as same as the gain fiber. The absorption coefficient at 2050 nm was measured to be approximately 0.22 dB/m for an 80-mW incidence power level, which is much lower than that of the Tm/Ho-codoped fiber. Since these two fibers have a comparable  $\text{Tm}^{3+}$  doping concentration, the 2050-nm laser energy in the Tm/Ho-codoped fiber SA is mainly absorbed by the  $\text{Ho}^{3+}$ . The maximum 2050-nm single-frequency laser power (and the corresponding pump power) with different SA lengths are summarized in Table 1. The experimental results using the same length of Tm/Ho-codoped fiber SA are also present for comparison. Using a Tm-doped fiber SA shorter than 2 m, stable single-frequency lasing was not possible and severe mode hopping was observed due to the weak dynamic Bragg grating. When the SA was extended to 4 m, the maximum single-frequency output power was 60 mW and improved to 93 mW as the length of the SA was further increased to 6 m. Compared with the aforementioned results where a Tm/Ho-codoped fiber was used as the SA, the single-frequency output power when using the same length of Tm-doped fiber exhibited an obvious drop. This behavior verified that the Tm/Ho-codoped fiber or Ho-doped fiber are more preferable choices of the SA to enhance the output power for a single-frequency fiber laser above 2  $\mu$ m.

Finally, it is worth discussing the influence of the energy transfer between  $\text{Tm}^{3+}$  and  $\text{Ho}^{3+}$  on the induced grating. The properties of the grating depend on the strength and period of the refractive index change along the SA, which originates from the different absorbance at nodes and antinodes. Since the overall absorption of the Tm/Ho-codoped fiber at 2050 nm is mainly contributed by the  $\text{Ho}^{3+}$ , the energy transfer from  $\text{Tm}^{3+}$  to  $\text{Ho}^{3+}$  is relatively weak. The formation of the dynamic Bragg grating mainly resulted from the  $\text{Ho}^{3+}$  ions and the energy transfer between  $\text{Tm}^{3+}$  and  $\text{Ho}^{3+}$  has a minor influence on the induced grating.

In conclusion, we have proposed and demonstrated a single-frequency Tm-doped fiber ring laser at 2050 nm by using a piece of Tm/Ho-codoped fiber as the SA. Compared with the  $\text{Tm}^{3+}$  ions, the  $\text{Ho}^{3+}$  ions exhibit a higher absorption at 2050 nm, enabling a stronger dynamic Bragg grating and mode selection capability. In experiment, the influence of the SA length on the single-frequency output was investigated in detail. The maximum single-frequency laser power was 215 mW with a slope efficiency in terms of launched pump power of 22%. This work paves a new way for a high-power single-frequency fiber oscillator operating in the wavelength region deviating from the gain peak of the active fiber.

**Funding.** National Natural Science Foundation of China (61975146, 62075159, 62105240); Major Scientific and Technological Innovation Projects of Key R&D Plans in Shandong Province (2019JZZY020206); The Shandong Province Taishan Industry Leading Talent Project (2020); Shandong Province Key R&D Program (2020CXGC010104); Science, Technology and Innovation Commission of Shenzhen Municipality (JSGG20201102152200001).

**Disclosures.** The authors declare no conflicts of interest.

**Data availability.** Data underlying the results presented in this paper are not publicly available at this time but may be obtained from the authors upon reasonable request.

## REFERENCES

- J. Wu, Y. Ju, T. Dai, B. Yao, and Y. Wang, *Opt. Express* **25**, 27671 (2017).
- T. J. Wagener, N. Demma, J. D. Kmetec, and T. S. Kubo, *IEEE Aerosp. Electron. Syst. Mag.* **10**, 23 (1995).
- F. Gibert, P. H. Flamant, D. Bruneau, and C. Loth, *Appl. Opt.* **45**, 4448 (2006).
- X. Guan, C. Yang, T. Qiao, W. Lin, Q. Zhao, G. Tang, G. Qian, Q. Qian, Z. Yang, and S. Xu, *Opt. Express* **26**, 6817 (2018).
- S. Fu, W. Shi, J. Lin, Q. Fang, Q. Sheng, H. Zhang, J. Wen, and J. Yao, *Opt. Lett.* **40**, 5283 (2015).
- W. Walasik, D. Traoré, A. Amavigan, R. E. Tench, J. M. Delavaux, and E. Pinsard, *J. Lightwave Technol.* **39**, 5096 (2021).
- L. Zhang, J. Zhang, Q. Sheng, C. Shi, W. Shi, and J. Yao, *Opt. Express* **29**, 27048 (2021).
- J. Zhang, Q. Sheng, L. Zhang, C. Shi, S. Sun, X. Bai, W. Shi, and J. Yao, *Opt. Express* **29**, 21409 (2021).
- J. Zhang, W. Yao, H. Wang, W. Zhou, X. Wu, and D. Shen, *IEEE Photon. Technol. Lett.* **31**, 1241 (2019).
- J. Zhang, Q. Sheng, L. Zhang, C. Shi, S. Sun, W. Shi, and J. Yao, *Adv. Photonics Res.* **3**, 2100256 (2022).
- S. Stepanov, *J. Phys. D: Appl. Phys.* **41**, 224002 (2008).
- K. Poozesh, K. Madinipour, and P. Parvin, *J. Lightwave Technol.* **36**, 4880 (2018).
- S. D. Lim, J. K. Yoo, and S. K. Kim, *IEEE Photonics J.* **8**, 1 (2016).
- C. Shi, S. Fu, G. Shi, S. Sun, Q. Sheng, W. Shi, and J. Yao, *Optik* **187**, 291 (2019).
- Y. Guo, F. Yan, T. Feng, Q. Qin, W. Han, D. Cheng, C. Yu, D. Yang, H. Zhou, and Y. Suo, *Infrared Phys. Technol.* **122**, 104058 (2022).
- N. Simakov, A. Hemming, W. A. Clarkson, J. Haub, and A. Carter, *Opt. Express* **21**, 28415 (2013).
- J. Geng, Q. Wang, T. Luo, S. Jiang, and F. Amzajerdian, *Opt. Lett.* **34**, 3493 (2009).